Jan Eliáš

HOMOGENIZATION OF DISCRETE MESOSCALE MODEL OF CONCRETE APPLIED TO COUPLED MECHANICS AND MASS TRANSPORT

BRNO UNIVERSITY OF TECHNOLOGY

Faculty of Civil Engineering

Institute of Structural Mechanics

Assoc. Prof. Ing. Jan Eliáš, Ph.D.

HOMOGENIZATION OF DISCRETE MESOSCALE MODEL OF CONCRETE APPLIED TO COUPLED MECHANICS AND MASS TRANSPORT

HOMOGENIZACE DISKRÉTNÍHO MESOÚROVŇOVÉHO MODELU BETONU PRO SDRUŽENOU ÚLOHU MECHANIKY A TRANSPORTU

THESIS OF A LECTURE FOR APPOINTMENT AS PROFESSOR
IN THE FIELD OF STRUCTURAL AND TRANSPORT ENGINEERING

VYSOKÉ UČENÍ NAKLADATELSTVÍ
TECHNICKÉ VUTIUM
V BRNĚ

BRNO 2022

KEYWORDS

discrete model; mesoscale; concrete; mechanics; fracture; diusion; mass transport; coupled problem; multiscale; multiphysics; computational homogenization; Cosserat continuum

KLÍČOVÁ SLOVA

diskrétní model; mesoúroveň; beton; mechanika; lom; difuze; transport; sdružená úloha; homogenizace; Cosseratovo kontinuum

Contents

About the Author (brief CV)

Jan Eliáš

Institute of Structural Mechanics

⌂ Faculty of Civil Engineering

Brno University of Technology

📍 Veveří 95, 602 00 Brno, Czech Republic

📞 +420 541 147 132

✉ jan.elias@vut.cz

🌐 https://www.fce.vutbr.cz/stm/elias.j

Academic degrees

- Doctoral degree (Ph.D.): Brno Univ. of Technology, Faculty of Civil Engineering, Inst. of Structural Mechanics, field *Constructions and Traffic Structures*, 2009.
- Associate Professor degree (doc.): Brno Univ. of Technology, Faculty of Civil Engineering, Inst. of Structural Mechanics, field *Constructions and Traffic Structures*, 2017.

Research interests

general mechanics of transient and steady state of solids; coupled multiphysical phenomena; variational principles; Monte Carlo integration; blending of probability and mechanics; soft computing techniques; optimization; mesoscale discrete models of concrete

Visiting positions

- 10 months with Henrik Stang at Technical University of Denmark, Denmark (2007-2008)
- 10 months with Zdeněk P. Bažant at Northwestern University, USA (2009-2011)
- three times 1–2 months with Jia-Liang Le at U. of Minnesota, USA (2012, 2014, 2016)
- 11 months with Gianluca Cusatis at Northwestern University, USA (2020-2021)

Students

- high school students: Jakub Koňárek (2020)
- bachelor students: Radek Dubina (2013), Josef Květoň (2013), Kateřina Bónová (2016), Martin Ladecký (2016, the main supervisor was Jan Novák from ČVUT), Monika Středulová (2018)
- master students: Radek Dubina (2014), Josef Květoň (2015), Kateřina Bónová (2017), Monika Středulová (2021, at Univ. of Porto), Beáta Fleischerová (2022)
- Ph.D. students: Jana Kaděrová (2018), Josef Květoň (2020)

Research projects

principal investigator of 3 research projects supported by the Czech Science Foundation and 1 project supported by the Czech Ministry of Education, Youth and Sports; member of several other project teams

Publications

Author and co-author of 23 papers in journals with impact factor and more than 40 conference papers, $\mathcal{H}$-index = 11 (WoS) 12 (Scopus)

1   Introduction

The long lasting research on mechanics of solids usually relies on the fundamental assumption about continuity of the displacement field. A major complication arises when *continuous* displacements are used to describe cracking, a phenomenon manifested by discrete displacement jumps. One can either weaken the discontinuity by assuming smeared cracks (e.g., crack band model [1]) or embed additional auxiliary discontinuities into the model (e.g., XFEM [2]).

Another complex issue related to fracture simulations of quasibrittle materials (such as concrete, rock, bone, ice, ceramics, ...) is regularization of the dissipated energy. The strain softening constitutive relation exhibited by these materials makes the mathematical boundary value problem ill-posed. The inelastic strain tends to localize into an infinitely thin line because it is, from the energetic point of view, the cheapest failure mode. The numerical solution therefore becomes spuriously dependent on the chosen approximation of the displacement field. The problem is magnified in *homogeneous* models that do not posses any information about material internal structure. The strain localization is in a real fracture process limited by the material heterogeneity which gives rise to a finite width region called the fracture process zone where the energy dissipation takes place. Therefore all remedies introduced in the numerical modeling to regularize the energy dissipation somehow reflect the internal material structure and introduce some length scale into the model. This can be for example nonlocal radius in integral nonlocal models [3] or length parameter in phase field models [4].

There is also a class of models that directly represents material heterogeneity and therefore contains the internal length scale automatically. In the case of concrete, these models are called *mesoscale* models because they reflect concrete mesostructure composed of mineral grains, matrix, pores and the interfacial transition zone. A huge disadvantage of mesoscale models is their computational burden. The spatial discretization needs to be fine enough to accommodate the material heterogeneities. Therefore even the medium size laboratory specimens might become computationally infeasible.

The computational cost of mesoscale models can be substantially reduced by *discrete* approximation of the displacement field. Several versions of discrete mesoscale models exist, the most prominent one is the Lattice Discrete Particle Model (LDPM) developed in Refs. [5, 6]. The kinematics of the model is based on polyhedral rigid bodies interconnected by compliant contacts. Each rigid body is generated by a special tessellation around one larger mineral grain, therefore the computational burden associated with the mesoscale structure is as low as possible. There is a vectorial constitutive relation at the interparticle contact lumping together both elastic and inelastic parts of the material behavior. Thanks to discrete displacement jumps between rigid particles in the discrete model, the cracks are naturally represented and oriented. LDPM has been proven to be robust and reliable numerical model, it has been extensively validated using large sets of experiments.

Durability of concrete structures is determined by chemical and physical degradation of the material. One of the major factors is transport of chemical substances inside or outside the structural domain in a form of liquid. The transport phenomenon is strongly coupled with mechanical behavior in the following three ways.

- The Biot's theory describes how the volumetric strain affects the fluid pressure and how the fluid pressure contributes to the stress state in solid.
- Open cracks create channels for the fluid to run through them significantly easier than through the intact material.
- Cracks provide free volume filled with fluid and therefore serve as storage units.

The first coupling fabric, the Biot's theory, can be easily implemented in any model type, however, the other two coupling schemes require detailed knowledge about the cracking pattern.

The *mesoscale discrete* models are ideal for coupled mechanical-transport problems because they provide high fidelity representation of both diffused and localized cracking states.

There are two major open issues concerning the mesoscale discrete models. The first and the most crucial is the computational complexity of the model when applied at a larger scale. This issue is common to all mesoscale models, the discrete version is actually the most efficient one. Several techniques reducing the burden have been proposed, e.g., adaptive discretization [7, 8], coarse graining [9], model order reduction via proper orthogonal decomposition [10, 11] and computational homogenization [12, 13]. The second issue is more theoretical, the discrete models cannot achieve all thermodynamically admissible values of Poisson's ratio. The upper limit is 0.25 in three dimensions. This fundamental limitation is caused by blending the volumetric and deviatoric deformation parts in the vectorial constitutive model. There are many papers showing how to improve discrete models towards achieving higher Poisson's ratio, e.g., Refs. [14, 15]. All of them essentially mimic the volumetric-deviatoric strain decomposition used in the continuum models. Unfortunately, the consequence is a loss of stress oscillations in the model that are understand to be arising from the mesostructure. The models are then, for example, not capable to exhibit splitting parallel cracks under compression. For these reasons, the remedies for unlimited Poisson's ratios are not popular in he mesoscale modeling community.

The research of Jan Eliáš, author of this thesis, has been largely directed towards mechanical mesoscale discrete modeling of concrete. Initially, he studied the lattice approach [16, 17], the focus soon shifted to the LDPM type of models. Papers [18, 19] are devoted to blending mechanics and spatial variability of material parameters using discrete LDPM type of model. The challenging question of Poisson's ratio limit is addressed in Ref. [20], related subject of a boundary layer (or a wall effect) is described in Ref. [21]. Finally, the reduction of computational cost by an adaptive technique is published in Ref. [22]. The recent publication [23] is a review paper about discrete modeling of quasibrittle fracture that was written in collaboration with arguably the best scholars from the field.

This thesis is based on the last two publications of the author [24, 25], both of them are now in a review process and both of them were created in collaboration with Gianluca Cusatis, creator of the LDPM model, during author's stay at Northwestern University in years 2020–2021. The primary objective of the papers is to reduce computational cost of mesoscale discrete models to allow their application in engineering practice. The first publication [24] describes asymptotic expansion homogenization of discrete model for mass transport in concrete, the second one [25] uses the same asymptotic expansion to develop a homogenized solution for coupled mechanical-mass transport mesoscale discrete model.

2   Mesoscale Discrete Model of Concrete

The discrete model of coupled mechanics and mass transport in fully saturated concrete is briefly described in this section, detailed information are available for interested reader in Ref. [25].

The spatial discretization of the domain is based on a computer-generated concrete mesostructure. Radii of the spherical particles are obtained from the Fuller curve [26]. The location of the particles in the domain is generated randomly in a sequence restricting overlapping. The power/Laguerre tessellation provides mass transport connectivity and discrete bodies for mechanics while the (weighted) Delaunay triangulation gives mechanical connectivity and its simplices serve as control volumes for the mass transport part. Such dual structure has been originally proposed by Grassl [27] in 2D end extended to 3D in Ref. [28]. Thanks to the duality

<center>intact configuration   cracked configuration</center>
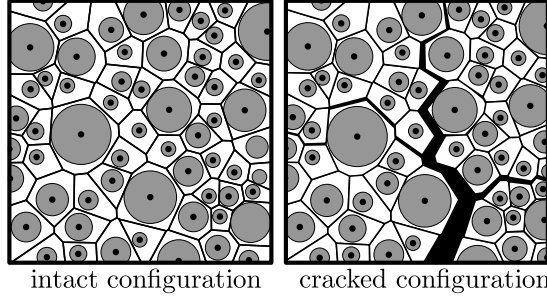
Figure 1: Idealization of the concrete mesoscale structure by the discrete model. Left: intact material, right: open cracks filled with the fluid.

of the mechanical and transport geometrical structure, the material permeability coefficient can be easily modified to account for crack openings in the mechanical part, see Fig. 1.

The mathematical structure of the coupled problem of mass transport and mechanics is described in Fig. 2. There are three unknown field sets, one of them is refered to as the primary one, the other two are dependent/secondary fields. The *primary* fields are the vector of displacements, $\mathbf{u}$, the vector of rotations, $\boldsymbol{\theta}$, and the pressure scalar, p. Displacement and rotation degrees of freedom (DoF) are defined at centers of the spherical inclusions (denoted I or J hereinafter) while the pressure DoF are defined at the vertices of the tessellation (denoted P and Q hereinafter). The first dependent field set is often called *intermediate* and involves the vector of strain, $\boldsymbol{\varepsilon}$, the vector of curvature, $\boldsymbol{\chi}$, and the scalar of pressure gradient, g. The last, dependent field set called *flux* collects the vector of traction, $\mathbf{t}$, the vector of couple traction, $\mathbf{m}$, and the flux scalar, j. The mechanical dependent variables are defined at the contact between the particles while the transport dependent variables are found at the contact between simplices (or control volumes). The set of know fields referred to as *sources* involves the vector of volume force, $\mathbf{b}$, the vector of volume moment, $\mathbf{z}$ (omitted in this work), and the scalar of fluid sources or sinks, q. Two basic types of boundary conditions are the *essential boundary conditions* prescribing the primary variables over some portion of the domain boundary explicitly and the *natural boundary conditions* prescribing the flux variables over the rest of the domain boundary.

Three set of equation called *kinematic*, *constitutive* and *balance* relate the unknown fields. Before deriving them, let us first present Fig. 3, where contacts between particles I and J
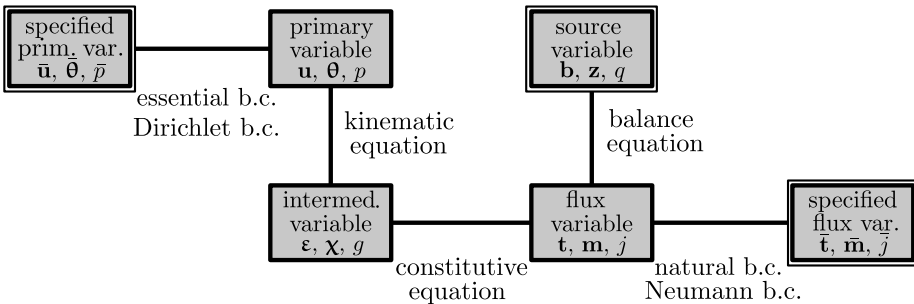
Figure 2: Tonti diagram showing structure of the multiphysical coupled problem of mass transport and mechanics.
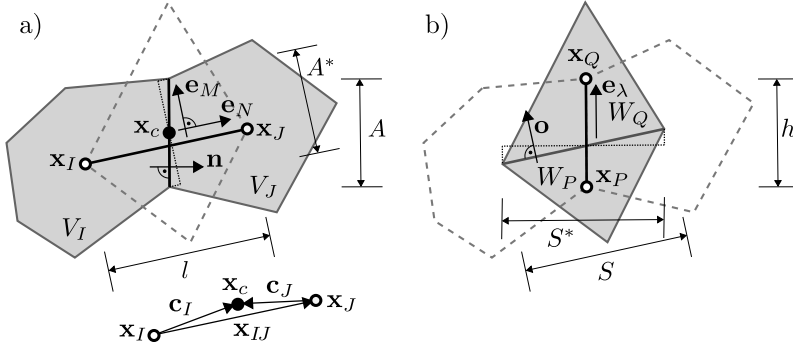
Figure 3: Two dimensional sketch of the mechanical (a) and conduit (b) elements created by a dual tessellation of the domain into ideally rigid mechanical particles and control volumes for the mass transport.

and between simplices P and Q are sketched in 2D. These contacts are called mechanical and conduit elements hereinafter. The strain and curvature at the contact between bodies I and J read

$$\varepsilon_\alpha = \frac{1}{l} \left(\mathbf{u}^J - \mathbf{u}^I + \boldsymbol{\mathcal{E}} : \left(\boldsymbol{\theta}^J \otimes \mathbf{c}_J - \boldsymbol{\theta}^I \otimes \mathbf{c}_I \right) \right) \cdot \mathbf{e}_\alpha \qquad\qquad \chi_\alpha = \frac{1}{l} \left(\boldsymbol{\theta}^J - \boldsymbol{\theta}^I \right) \cdot \mathbf{e}_\alpha \qquad (1)$$

where $\mathbf{c}$ is a vector connecting particle governing node with the integration point $\mathbf{x}_c$ at the contact face, $\boldsymbol{\mathcal{E}}$ is Levi-Civita permutation symbol and $\mathbf{e}_\alpha$ are local normal and two tangential directions ($\alpha \in \{N, M, L\}$), respectively. The length of the contact is $l = ||\mathbf{x}_{IJ}||$ and the contact direction $\mathbf{e}_N = \mathbf{x}_{IJ}/l$ where $\mathbf{x}_{IJ} = \mathbf{x}_J - \mathbf{x}_I$. The contact direction $\mathbf{e}_N$ can be in general different from the true face normal $\mathbf{n}$. The contact area A is therefore projected as $A^\star = A\mathbf{e}_N \cdot \mathbf{n}$ to account for directional mismatch.

The conduit element has area S, normal $\mathbf{o}$, length $h = ||\mathbf{x}_{PQ}||$ and contact direction $\mathbf{e}_\lambda = \mathbf{x}_{PQ}/h$, where $\mathbf{x}_{PQ} = \mathbf{x}_Q - \mathbf{x}_P$. The situation is sketched in 2D in Fig. 3b. Estimation of pressure gradient between two nodes yields the last kinematic equation

$$g = \nabla p \cdot \mathbf{e}_\lambda \approx \frac{p^Q - p^P}{h} \qquad (2)$$

The transport face normal $\mathbf{o}$ might not be parallel to the contact vector $\mathbf{e}_\lambda$ as well. Projected area $S^\star = S\mathbf{o} \cdot \mathbf{e}_\lambda$ is again introduced to account for the directional mismatch when the total flux is computed later in Eq. (5). Both Voronoi and power/Laguerre tessellation actually ensure parallelisms $\mathbf{e}_N||\mathbf{n}$ and $\mathbf{e}_\lambda||\mathbf{o}$ but the general formulation with projected areas $A^\star$ and $S^\star$ is used for sake of generality.

The second set of equations are constitutive equations which provide flux variables.

$$j = f_j(p_\lambda, g, \delta_\lambda) = -\lambda(p_\lambda, \delta_\lambda)g \qquad\qquad \mathbf{t} = f_s\left(\boldsymbol{\varepsilon}\right) - bp_a\mathbf{e}_N \qquad\qquad \mathbf{m} = f_m\left(\boldsymbol{\chi}\right) \qquad (3)$$

The first equation expresses linear dependence of the flux, j, on the pressure gradient, g, while the permeability coefficient, λ, is governed by an average crack opening, δ_λ, and an average pressure, p_λ, in the element. Several possible formulations are being used to describe effects of cracks or pressure on material permeability in the literature [29, 30, 31]. The second constitutive equation defines another coupling between transport and mechanics as the total traction, $\mathbf{t}$, becomes dependent on the fluid pressure according to Biot's theory [32, 33], b

is a material parameter called Biot coefficient and $\mathbf{s} = f_s(\boldsymbol{\varepsilon})$ is the traction vector in the solid. The pressure p_a is the weighted average pressure from control volumes surrounding the mechanical element. The third constitutive equation assumes that the couple traction, $\mathbf{m}$, depends solely on the curvature, $\boldsymbol{\chi}$, i.e., it is decoupled from the transport part of the model. The homogenization procedure described in this thesis is in principle independent on the choice of the functions λ, f_s and f_m. Implementation of the constitutive equations employs simplified relations developed for the LDPM model [34]. They are stated in Ref. [25] along with material parameters used in the numerical examples.

Finally, balance equations are assembled. The balance of linear and angular momentum of particle I read

$$V\rho\ddot{\mathbf{u}}^I + \mathbf{M}_{u\theta} \cdot \ddot{\boldsymbol{\theta}}^I - V\mathbf{b} = \sum_J A^\star t_\alpha \mathbf{e}_\alpha \qquad \mathbf{M}_\theta \cdot \ddot{\boldsymbol{\theta}}^I + \mathbf{M}_{u\theta}^T \cdot \ddot{\mathbf{u}}^I = \sum_J A^\star[\mathbf{w} + m_\alpha \mathbf{e}_\alpha] \qquad (4)$$

where $\mathbf{w} = \boldsymbol{\mathcal{E}} : (\mathbf{c}_I \otimes \mathbf{t}) = t_\alpha \boldsymbol{\mathcal{E}} : (\mathbf{c}_I \otimes \mathbf{e}_\alpha)$ is the moment of traction with respect to the mechanical node $\mathbf{x}_I$. $\mathbf{M}_\theta$ and $\mathbf{M}_{u\theta}$ are the moment of inertia tensors and V is a volume of the rigid body.

The mass balance equation for a fully saturated medium, established for each control volume P separately, reads

$$\sum_{Q \in W} \left[S^\star j - \rho_{w0} W \dot{v}_c \left(1 + b + \frac{p_\lambda - p_0}{K_w} \right) - \rho_{w0} W v_c \frac{\dot{p}_\lambda}{K_w} \right] - \rho_{w0} \left(3b\dot{\varepsilon}_V + \frac{\dot{p}_\lambda}{M_b} \right) W - Wq = 0 \tag{5}$$

It is assumed that the liquid is slightly compressible with bulk modulus K_w, ρ_{w0} is fluid density under the reference pressure, p_0. M_b is the Biot modulus (reciprocal of capacity, c), W is volume of the control volume (tetrahedron), the volumetric strain, ϵ_V, is estimated as one third of the relative difference in a tetrahedron volume due to displacements $\mathbf{u}$, v_c is the relative crack volume within a conduit element connecting nodes P and Q evaluated as the total crack volume in the element divided by the element volume.

3 Asymptotic Expansion

Two spatial variables are considered now for every point in the domain: the macroscopic, slow variable $\mathbf{x}$ and the microscopic, fast variable $\mathbf{y}$ (see Fig. 4). The following scale separation relationship holds

$$\mathbf{x} = \eta\mathbf{y} \tag{6}$$
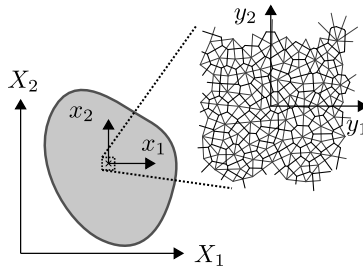
Figure 4: Reference systems considered in the asymptotic expansion homogenization.

with η being the separation of scales constant with properties $0 < \eta \ll 1$. The model appears continuous from the viewpoint of reference system $\mathbf{x}$ but discrete in the reference system $\mathbf{y}$.

Moreover, another global reference system $\mathbf{X}$ that uniquely defines position in the continuous macroscopic space is introduced. System $\mathbf{X}$ has the same units as $\mathbf{x}$ but there is only one such system while infinitely many $\mathbf{x}$ reference systems are defined at macroscopic spatial points.

All the variables involving length are consider to be in the $\mathbf{x}$ reference system. One needs to transfer them into the $\mathbf{y}$ reference system according to the transformation rules reflecting the power of distance unit involved. $\tilde{\bullet}$ denotes variable $\bullet$ in $\mathbf{y}$ reference system.

The primary variables p, $\mathbf{u}$ and $\boldsymbol{\theta}$ are now considered to be approximated by two components, the macroscopic component $\bullet^{(0)}$ and the microscopic component $\bullet^{(1)}$. Expansions of the pressure and displacements are straightforward. The expansion of rotations is done according to Rezakhani and Cusatis [12] by assuming existence of some continuous displacement-like field $\mathbf{d}$ the curl of which provides the rotations.

$$p(\mathbf{X}, \mathbf{y}) = p^{(0)}(\mathbf{X}, \mathbf{y}) + \eta p^{(1)}(\mathbf{X}, \mathbf{y}) + \dots \tag{7a}$$

$$\mathbf{u}(\mathbf{X}, \mathbf{y}) = \mathbf{u}^{(0)}(\mathbf{X}, \mathbf{y}) + \eta \mathbf{u}^{(1)}(\mathbf{X}, \mathbf{y}) + \dots \tag{7b}$$

$$\boldsymbol{\theta}(\mathbf{X}, \mathbf{y}) = \eta^{-1} \boldsymbol{\omega}^{(-1)}(\mathbf{X}, \mathbf{y}) + \boldsymbol{\omega}^{(0)}(\mathbf{X}, \mathbf{y}) + \boldsymbol{\varphi}^{(0)}(\mathbf{X}, \mathbf{y}) + \eta \boldsymbol{\varphi}^{(1)}(\mathbf{X}, \mathbf{y}) + \dots \tag{7c}$$

All of the fields p, $\mathbf{u}$ and $\mathbf{d}$ are assumed to be periodic over some Representative Volume Element (RVE) with periodic geometrical structure of the discrete model. Therefore also the rotations $\boldsymbol{\omega}$ and $\boldsymbol{\varphi}$ derived from $\mathbf{d}$ must be RVE-periodic. It is also assumed that all these fast fields (or fluctuations) yield zero average over the RVE.

From the viewpoint of the macroscopic spatial coordinate $\mathbf{X}$, neighboring mechanical nodes I and J are close to each other. According to Fish et al. [35], one can use the macroscopic gradient ∇_X at node I to approximate the mechanical field variables at node J. The same Taylor expansion of pressure around node P provides pressure estimation at neighboring node Q.

$$p(\mathbf{X}_Q, \mathbf{y}_Q) = p(\mathbf{X}_P, \mathbf{y}_Q) + \frac{\partial p(\mathbf{X}_P, \mathbf{y}_Q)}{\partial X_i} x_i^{PQ} + \frac{1}{2} \frac{\partial^2 p(\mathbf{X}_P, \mathbf{y}_Q)}{\partial X_i X_j} x_i^{PQ} x_j^{PQ} + \mathcal{O}(h^3) \tag{8a}$$

$$\mathbf{u}(\mathbf{X}_J, \mathbf{y}_J) = \mathbf{u}(\mathbf{X}_I, \mathbf{y}_J) + \frac{\partial \mathbf{u}(\mathbf{X}_I, \mathbf{y}_J)}{\partial X_j} x_j^{IJ} + \frac{1}{2} \frac{\partial^2 \mathbf{u}(\mathbf{X}_I, \mathbf{y}_J)}{\partial X_j X_k} x_j^{IJ} x_k^{IJ} + \mathcal{O}(l^3) \tag{8b}$$

$$\boldsymbol{\theta}(\mathbf{X}_J, \mathbf{y}_J) = \boldsymbol{\theta}(\mathbf{X}_I, \mathbf{y}_J) + \frac{\partial \boldsymbol{\theta}(\mathbf{X}_I, \mathbf{y}_J)}{\partial X_j} x_j^{IJ} + \frac{1}{2} \frac{\partial^2 \boldsymbol{\theta}(\mathbf{X}_I, \mathbf{y}_J)}{\partial X_j X_k} x_j^{IJ} x_k^{IJ} + \mathcal{O}(l^3) \tag{8c}$$
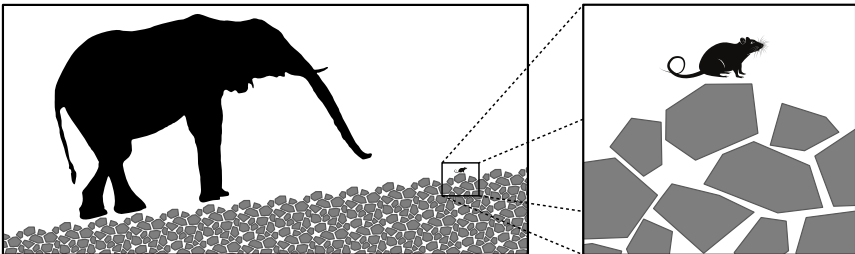
Figure 5: An analogy to homogenization: we are interested in an elephant point of view (reference system $\mathbf{X}$), a mouse point of view (reference system $\mathbf{y}$) is understood as quasi-periodic oscillations equal on average to the mean behavior observed by the elephant.

Terms with h^3 and l^3 are omitted as h and l are assumed to be very small with respect to the global variable $\mathbf{X}$.

The compatibility equations (1) and (2) are now rewritten

$$g = \frac{1}{h} \left[p(\mathbf{X}_Q, \mathbf{y}_Q) - p(\mathbf{X}_P, \mathbf{y}_P) \right] \tag{9a}$$

$$\varepsilon_\alpha = \frac{1}{l} \left[\mathbf{u}(\mathbf{X}_J, \mathbf{y}_J) - \mathbf{u}(\mathbf{X}_I, \mathbf{y}_I) + \boldsymbol{\mathcal{E}} : (\boldsymbol{\theta}(\mathbf{X}_J, \mathbf{y}_J) \otimes \mathbf{c}_J - \boldsymbol{\theta}(\mathbf{X}_I, \mathbf{y}_I) \otimes \mathbf{c}_I) \right] \cdot \mathbf{e}_\alpha \tag{9b}$$

$$\chi_\alpha = \frac{1}{l} \left[\boldsymbol{\theta}(\mathbf{X}_J, \mathbf{y}_J) - \boldsymbol{\theta}(\mathbf{X}_I, \mathbf{y}_I) \right] \cdot \mathbf{e}_\alpha \tag{9c}$$

and the Taylor series (8) as well as the asymptotic expansion (7) is substituted afterwards. Note that thanks to the Taylor expansion, there is always the same $\mathbf{X}$ coordinate (either $\mathbf{X}_P$ or $\mathbf{X}_I$) denoting the RVE location. The equations must hold for any $\mathbf{X}$ coordinate (or any RVE), therefore we can drop it for sake of simplicity. As long as only a single RVE is involved (constant $\mathbf{X}$ coordinate) the notation can be simplified to $\bullet^{\alpha P} = \bullet^{(\alpha)}(\mathbf{X}, \mathbf{y}_P)$

The set of compatibility equations with substituted (7) and (8) and scaled length variables reads

$$g = \eta^{-1} g^{(-1)} + g^{(0)} + \eta g^{(1)} + \dots \tag{10a}$$

$$\varepsilon_\alpha = \eta^{-1} \varepsilon_\alpha^{(-1)} + \varepsilon_\alpha^{(0)} + \eta \varepsilon_\alpha^{(1)} + \dots \tag{10b}$$

$$\chi_\alpha = \eta^{-2} \chi_\alpha^{(-2)} + \eta^{-1} \chi_\alpha^{(-1)} + \chi_\alpha^{(0)} + \dots \tag{10c}$$

where the respective components can be easily derived from the above expansion structure. The terms with higher η power are omitted as they are negligibly small.

Next, the volumetric strain, ε_V, average normal crack opening, δ_N, and cracks volume density, v_c, are expanded. The exact expressions are not important at this point, but the scale (power of η) at which they appear is.

$$\varepsilon_V = \eta^{-1} \varepsilon_V^{(-1)} + \varepsilon_V^{(0)} + \eta \varepsilon_V^{(1)} + \dots \tag{11a}$$

$$\delta_N = \delta_N^{(0)} + \eta \delta_N^{(1)} + \eta^2 \delta_N^{(2)} + \dots \tag{11b}$$

$$v_c = \eta^{-1} v_c^{(-1)} + v_c^{(0)} + \eta^1 v_c^{(1)} + \dots \tag{11c}$$

Finally, the stress-like variables flux, traction, couple traction and moment of traction are also decomposed into

$$j = \eta^{-1} j^{(-1)} + j^{(0)} + \eta j^{(1)} + \dots \qquad\qquad \mathbf{t} = \eta^{-1} \mathbf{t}^{(-1)} + \mathbf{t}^{(0)} + \eta \mathbf{t}^{(1)} + \dots \tag{12a}$$

$$\mathbf{m} = \mathbf{m}^{(0)} + \eta \mathbf{m}^{(1)} + \eta^2 \mathbf{m}^{(2)} + \dots \qquad\qquad \mathbf{w} = \mathbf{w}^{(0)} + \eta \mathbf{w}^{(1)} + \eta^2 \mathbf{w}^{(2)} + \dots \tag{12b}$$

The first terms in expansion (12) are expressed by components of the constitutive relations (3) with the lowest η powers

$$\eta^{-1} j^{(-1)} = -\eta^{-1} \lambda \left(p_\lambda^{(0)}, \delta_\lambda^{(0)} \right) g^{(-1)} \qquad\qquad \eta^{-1} \mathbf{t}^{(-1)} = f_s \left(\eta^{-1} \boldsymbol{\varepsilon}^{(-1)} \right) - \eta^{-1} p_a^{(-1)} b \mathbf{e}_N \tag{13a}$$

$$\mathbf{m}^{(0)} = f_m \left(\eta^{-2} \boldsymbol{\chi}^{(-2)} \right) \qquad\qquad \mathbf{w}^{(0)} = \eta^{-1} t_\alpha^{(-1)} \boldsymbol{\mathcal{E}} : (\mathbf{c}_I \otimes \mathbf{e}_\alpha) \tag{13b}$$

The field $p^{(-1)}$ is always zero [25] and is introduced only because it is included in Eq. (13a). It will also be derived in the next Section that the primary fields $p^{(0)}$ and $\mathbf{u}^{(0)}$ are constant over the RVE and the primary field $\eta^{-1} \boldsymbol{\omega}^{(-1)}$ is zero. It further implies that

$$g^{(-1)} = j^{(-1)} = 0 \qquad \boldsymbol{\varepsilon}^{(-1)} = \mathbf{t}^{(-1)} = \mathbf{0} \qquad \boldsymbol{\chi}^{(-2)} = \mathbf{m}^{(0)} = \mathbf{0} \qquad \mathbf{w}^{(0)} = \mathbf{0} \tag{14}$$

Moreover, this lead us to the conclusion that the volumetric strain $\varepsilon_V^{(-1)}$, crack opening $\delta_\lambda^{(0)}$ and relative crack volume $v_c^{(-1)}$ are zero as well because they depend on the strain $\boldsymbol{\varepsilon}^{(-1)}$.

The second terms in expansion (12) are therefore again obtained from nonzero components with the lowest η power

$$j^{(0)} = -\lambda\left(p_\lambda^{(0)}, \eta\delta_\lambda^{(1)}\right)g^{(0)} \qquad\qquad \mathbf{t}^{(0)} = f_s\left(\boldsymbol{\varepsilon}^{(0)}\right) - p_a^{(0)}b\mathbf{e}_N \tag{15a}$$

$$\eta\mathbf{m}^{(1)} = f_m\left(\eta^{-1}\boldsymbol{\chi}^{(-1)}\right) \qquad\qquad \eta\mathbf{w}^{(1)} = t_\alpha^{(0)}\boldsymbol{\mathcal{E}} : (\mathbf{c}_I \otimes \mathbf{e}_\alpha) \tag{15b}$$

These equations represent the actual constitutive equations of the discrete model.

The third components of stress-like variables are approximated by the Taylor expansion. The flux (or more precisely the permeability coefficient λ) is expanded around points $p = p_\lambda^{(0)}$, $\delta_N = \eta\delta_\lambda^{(1)}$, traction $\mathbf{t}$ and moment of traction $\mathbf{w}$ around points $\boldsymbol{\varepsilon} = \boldsymbol{\varepsilon}^{(0)}$, $p = p_a^{(0)}$ and couple traction $\mathbf{m}$ around point $\boldsymbol{\chi} = \eta^{-1}\boldsymbol{\chi}^{(-1)}$, respectively.

The source terms q and $\mathbf{b}$ (as well as other variables, e.q., Biot coefficient b, capacity c or density ρ) might also be dependent on the primary or other fields. In such cases, their expansion must be developed as well and added to the balance equations in the next section.

4 Balance Equations at Multiple Scales

The balance equations of individual grains are now assembled using variables transformed into the $\mathbf{y}$ reference system. Starting with Eqs. (4) and (5), assuming all material parameters are of order $\approx \mathcal{O}(\eta^0)$, transforming all the length variables from $\mathbf{x}$ to $\mathbf{y}$ reference system, and dividing everything by η^3, η^3 or η^4, respectively, the balance equations read

$$\rho_{w0}\tilde{W}\left(3b\dot{\varepsilon}_V + \frac{\dot{p}_\lambda}{M_b}\right) + \tilde{W}q = \frac{1}{\eta}\sum_{Q \in W}\left[\tilde{S}^\star j - \eta\rho_{w0}\tilde{W}\dot{v}_c\left(1 + b + \frac{p_\lambda - p_0}{K_w}\right) - \eta\rho_{w0}\tilde{W}v_c\frac{\dot{p}_\lambda}{K_w}\right] \tag{16a}$$

$$\tilde{V}\rho\ddot{\mathbf{u}}^I + \eta\tilde{\mathbf{M}}_{u\theta} \cdot \ddot{\boldsymbol{\theta}}^I - \tilde{V}\mathbf{b} = \frac{1}{\eta}\sum_J \tilde{A}^\star t_\alpha \tag{16b}$$

$$\eta\tilde{\mathbf{M}}_\theta \cdot \ddot{\boldsymbol{\theta}}^I + \tilde{\mathbf{M}}_{u\theta}^T \cdot \ddot{\mathbf{u}}^I = \frac{1}{\eta^2}\sum_J \tilde{A}^\star(\mathbf{w} + m_\alpha\mathbf{e}_\alpha) \tag{16c}$$

The expansions developed in Eqs. (7), (10), (11) and (12) can now be substituted into the balance equations, which can be then decomposed into separate equation sets collecting the terms with corresponding powers of η.

η^{-2}: constant pressure $p^{(0)}$ and displacement $\mathbf{u}^{(0)}$

Terms with the negative second power of η brought back to the $\mathbf{x}$ reference system and multiplied by η^3, η^3 and η^4, respectively, yield

$$\eta^{-1}\sum_{Q \in W}S^\star j^{(-1)} = 0 \qquad \eta^{-1}\sum_{J \in V}A^\star t_\alpha^{(-1)}\mathbf{e}_\alpha = \mathbf{0} \qquad \sum_{J \in V}A^\star\left(\mathbf{w}^{(0)} + m_\alpha^{(0)}\mathbf{e}_\alpha\right) = \mathbf{0} \tag{17}$$

Assume now linear behavior only. Assembling these three equations for all particles and control volumes inside the RVE and considering the periodic boundary conditions, we obtain linear system with degrees of freedom $p^{(0)}$, $\mathbf{u}^{(0)}$ and $\eta^{-1}\boldsymbol{\omega}^{(-1)}$.

The first equation is satisfied in linear regime only if $p^{(0)}$ is constant over the whole RVE. Therefore, pressure gradients $g^{(-1)}$ and fluxes $j^{(-1)}$ are always zero. The solution to the third equation is constant $\eta^{-1}\boldsymbol{\omega}^{(-1)}$ providing $\boldsymbol{\chi}^{(-2)} = \mathbf{m}^{(0)} = \mathbf{0}$. Note that this solution was previously assumed in Eqs. (14). From constantness of $\eta^{-1}\boldsymbol{\omega}^{(-1)}$, one derives that the solution to the second balance equation (angular momentum) must correspond to a rigid body translation and rotation. The $\mathbf{u}^{(0)}$ can be expressed as $\mathbf{u}^{(0)}(\mathbf{X}, \mathbf{x}) = \mathbf{v}^{(0)}(\mathbf{X}) + \eta^{-1}\boldsymbol{\mathcal{E}} : \left(\boldsymbol{\omega}^{(-1)}(\mathbf{X}) \otimes \mathbf{x}\right)$. Such a rigid body rotation is developed in Ref. [12] for homogenization of the mechanical model. However, considering also the required y-periodicity of the unknown fields, the solution from from Ref. [12] is corrected here. Rotation $\eta^{-1}\boldsymbol{\omega}^{(-1)}$ must be zero rendering displacement $\mathbf{u}^{(0)}$ constant over the RVE.

Other solutions might exist in the nonlinear regime. However, the presented trivial solution to system (17) is always valid. The variables $p^{(0)}$ and $\mathbf{u}^{(0)}$ remain unknown. They represent the macroscopic pressure and macroscopic translation. Thanks to constantness of $p^{(0)}$ over the RVE, one may replace the averages of the pressure by constant: $p_\lambda^{(0)} = p_a^{(0)} = p^{(0)}$ hereinafter.

η^{-1}: RVE problem

Negative first power of η collects the following terms (already transformed to $\mathbf{x}$ reference system and multiplied by η^3, η^3 and η^4, respectively and with substituted solution from the previous section $v_c^{(-1)} = \varepsilon_V^{(-1)} = 0$).

$$\sum_{Q \in W} S^\star j^{(0)} = 0 \tag{18a}$$

$$\sum_{J \in V} A^\star s_\alpha^{(0)} \mathbf{e}_\alpha = p^{(0)} \sum_{J \in V} A^\star b \mathbf{e}_N \tag{18b}$$

$$\sum_{J \in V} A^\star \left(s_\alpha^{(0)} \mathbf{e}_\alpha \boldsymbol{\mathcal{E}} : (\mathbf{c}_I \otimes \mathbf{e}_N) + \eta m_\alpha^{(1)} \mathbf{e}_\alpha \right) = p^{(0)} \boldsymbol{\mathcal{E}} : \sum_{J \in V} A^\star b \mathbf{c}_I \otimes \mathbf{e}_N \tag{18c}$$

The pressure gradients, strains and curvatures that give rise to fluxes, tractions, couple tractions and moments of tractions are $g^{(0)}$, $\boldsymbol{\varepsilon}^{(0)}$ and $\eta^{-1}\boldsymbol{\chi}^{(-1)}$. Their expressions are rewritten based on the previous solution at η^{-2} scale ($\eta^{-1}\boldsymbol{\omega}^{(-1)} = \mathbf{0}$, $\mathbf{u}^{(0)}$ and $p^{(0)}$ are constant) and using identity $\mathbf{y}_{IJ} = \tilde{\mathbf{c}}_I - \tilde{\mathbf{c}}_J$ (Fig. 3b)

$$g^{(0)} = \frac{\eta}{h} \left[p^{1Q} - p^{1P} \right] - \hat{g} \tag{19a}$$

$$\varepsilon_\alpha^{(0)} = \frac{e_i^\alpha}{l} \left[\eta u_i^{1J} - \eta u_i^{1I} + \mathcal{E}_{ijk}\omega_j^{0J} c_k^J - \mathcal{E}_{ijk}\omega_j^{0I} c_k^I \right] - \hat{\varepsilon}_\alpha \tag{19b}$$

$$\eta^{-1}\chi_\alpha^{(-1)} = \frac{e_i^\alpha}{l} \left[\omega_i^{0J} - \omega_i^{0I} \right] \tag{19c}$$

These are original compatibility equations of the discrete model (1) and (2) with additional terms interpreted as eigen-pressure gradient $\hat{g}$ and eigen-strain $\hat{\boldsymbol{\varepsilon}}_\alpha$. These eigen terms turn out to be negative projections of the macroscopic pressure gradient $\mathbf{a} = \nabla_X p^{(0)}$ and the Cosserat strain tensor $\boldsymbol{\gamma} = \nabla_X \otimes \mathbf{u}^{(0)} - \boldsymbol{\mathcal{E}} \cdot \boldsymbol{\varphi}^{(0)}$

$$\hat{g} = -\frac{\partial p^{(0)}}{\partial X_i} e_i^\lambda = -\mathbf{a} \cdot \mathbf{e}_\lambda \tag{20a}$$

$$\hat{\varepsilon}_\alpha = -e_i^\alpha \left[\frac{\partial u_i^{(0)}}{\partial X_k} - \mathcal{E}_{ijk}\varphi_j^{(0)} \right] e_k^N = -\mathbf{e}_N \cdot \boldsymbol{\gamma} \cdot \mathbf{e}_\alpha \tag{20b}$$

Both vector $\mathbf{a}$ and tensor $\boldsymbol{\gamma}$ are provided by the macroscopic problem to be described later. Vector $\boldsymbol{\varphi}^{(0)}$ shall be identified from its definition as a macroscopic rotation of the RVE and therefore is constant over the RVE. The projection of the macroscopic Cosserat curvature that was derived in Ref. [12] is missing here since the $\boldsymbol{\omega}^{(-1)}$ term is corrected to be zero.

All three balance equations (18) to be solved numerically are steady state (or static) equations; the transient terms are not present. Unknown fields in these problems are $\eta p^{(1)}$, $\eta \mathbf{u}^{(1)}$ and $\boldsymbol{\omega}^{(0)}$ being the microscopic pressure, translation and rotation, respectively. Note that these problems are partially decoupled. The mechanical RVE depends only on the macroscopic pressure $p^{(0)}$, primary field $\eta p^{(1)}$ has no effect on the mechanical behavior. The transport problem, however, depends on mechanical primary field $\eta \mathbf{u}^{(1)}$ via the crack opening $\eta \delta_N^{(1)}$. One should therefore first solve the mechanical RVE problem and then use the computed crack openings $\eta \delta_N^{(1)}$ when solving the transport RVE problem.

The transport RVE is loaded only by the projection of the macroscopic pressure gradient in the form of eigen-pressure gradient (Eq. 20a). The load applied to the mechanical RVE comes from the macroscale in two ways: (i) in the form of eigen-strain (Eq. 20b) and (ii) as a force and moment acting on each particle due to the macroscopic fluid pressure as the right-hand side terms in Eqs. (18).

The periodic boundary conditions must be enforced for pressure, displacements and rotations. Furthermore, equations (19) consider only differences in the primary fields of displacements and pressure and are ill-conditioned without an additional constraint. The assumption behind the asymptotic expansion (7) requires the microscopic fields (fluctuations) to be zero on average, therefore the last boundary conditions should prescribe zero volumetric average of these fields over the RVE

$$\langle \eta p^{(1)} \rangle = 0 \qquad\qquad \langle \eta \mathbf{u}^{(1)} \rangle = \mathbf{0} \qquad\qquad (21)$$

where the weighted volumetric average reads

$$\langle \bullet \rangle = \frac{1}{V_0} \sum_{w \in V_0} V_w \bullet \qquad\qquad (22)$$

with V_w being volume (V_I or W_P) associated with the mechanical or mass transport node and w denotes either mechanical (e) or conduit (d) elements.

Direct enforcement of boundary conditions (21) is not practical. If one applies the linear constraint, the system matrix becomes full and computational and storage requirements rapidly grow. It is therefore recommended to randomly pick some node where pressure and translations are directly prescribed to be some random values (the easiest is to set everything to zero). After the solution is found, both transport and mechanical fast fields can be shifted to satisfy the required constraint, i.e., equations (21) are enforced during the post-processing. Moreover, the actual fast primary fields are typically not required and one can skip this post-processing step.

η^0: macroscopic level

Terms with zero power of η, already transformed to $\mathbf{x}$ reference system and multiplied by η^3, η^3 and η^4, respectively, are the following (note that terms with $v_c^{(1)}$, which is always zero, are

already deleted)

$$3b\dot{\varepsilon}_V^{(0)} + \frac{\dot{p}^{(0)}}{M_b} + q = \sum_{Q \in W} \left[\frac{\eta S^\star j^{(1)}}{W \rho_{w0}} - \dot{v}_c^{(0)} \left(1 + b + \frac{p^{(0)} - p_0}{K_w} \right) - v_c^{(0)} \frac{\dot{p}^{(0)}}{K_w} \right] \quad (23a)$$

$$\eta \sum_{J \in V} A^\star t_\alpha^{(1)} = V \rho \ddot{\mathbf{u}}^{0I} - V \mathbf{b} \quad (23b)$$

$$\eta^2 \sum_{J \in V} A^\star \left(\mathbf{w}^{(2)} + m_\alpha^{(2)} \mathbf{e}_\alpha \right) = \mathbf{M}_{u\theta}^T \cdot \ddot{\mathbf{u}}^{(0)} \quad (23c)$$

The equilibrium of the whole RVE unit is of interest at the macrolevel, therefore equations for all the bodies within the RVE are summed and divided by the RVE volume. In the case of forces and fluxes, the summations are straightforward. In the case of balance of moments (23c), one must select some reference point in the global coordinate system $\mathbf{X}$ and sum all the moment contributions with respect to that particular point. After several rigorous mathematical operations (details available in Ref. [25]), the summed equations transforms into the following partial differential equations for the poromechanical macroscale problem

$$\nabla_X \cdot \mathbf{f} = \rho_{w0} \left[\dot{v}_{c0} \left(1 + b + \frac{p^{(0)} - p_0}{K_w} \right) + v_{c0} \frac{\dot{p}^{(0)}}{K_w} + 3b\dot{\varepsilon}_V^{(0)} + \frac{\dot{p}^{(0)}}{M_b} \right] + q \quad (24a)$$

$$\nabla_X \cdot \boldsymbol{\sigma}_s - \nabla_X p^{(0)} \cdot \boldsymbol{\xi} = \langle \rho \rangle \ddot{\mathbf{u}}^{(0)} - \mathbf{b} \quad (24b)$$

$$\nabla_X \cdot \boldsymbol{\mu}_s - \nabla_X p^{(0)} \cdot \boldsymbol{\zeta} + \boldsymbol{\mathcal{E}} : \boldsymbol{\sigma}_s - p^{(0)} \boldsymbol{\mathcal{E}} : \boldsymbol{\xi} = \mathbf{0} \quad (24c)$$

where v_{c0} is the relative crack volume in the whole RVE. The remaining five new tensors represent outcome of the RVE problem sent back to the macrolevel; $\mathbf{f}$ is the flux vector, $\boldsymbol{\sigma}_s$ is the solid stress tensor, $\boldsymbol{\mu}_s$ is the solid couple stress tensor and $\boldsymbol{\xi}$ and $\boldsymbol{\zeta}$ are second order tensors describing RVE internal structure used to compute effect of pressure on the macroscopic stress and couple stress.

$$\mathbf{f} = \frac{1}{V_0} \sum_{d \in V_0} h S^\star j^{(0)} \mathbf{e}_\lambda \quad (25a)$$

$$\boldsymbol{\sigma}_s = \frac{1}{V_0} \sum_{e \in V_0} l A^\star s_\alpha^{(0)} \mathbf{e}_N \otimes \mathbf{e}_\alpha \quad (25b)$$

$$\boldsymbol{\mu}_s = \frac{1}{V_0} \sum_{e \in V_0} l A^\star \mathbf{e}_N \otimes \left[\eta m_\alpha^{(1)} \mathbf{e}_\alpha + s_\alpha^{(0)} \boldsymbol{\mathcal{E}} : (\mathbf{x}_c \otimes \mathbf{e}_\alpha) \right] \quad (25c)$$

$$\boldsymbol{\xi} = \frac{1}{V_0} \sum_{e \in V_0} l A^\star b \mathbf{e}_N \otimes \mathbf{e}_N \quad (25d)$$

$$\boldsymbol{\zeta} = \frac{1}{V_0} \sum_{e \in V_0} l A^\star b \mathbf{e}_N \otimes \left[\boldsymbol{\mathcal{E}} : (\mathbf{x}_c \otimes \mathbf{e}_N) \right] \quad (25e)$$

As the RVE geometry remains unchanged during calculation, $\boldsymbol{\xi}$ and $\boldsymbol{\zeta}$ are constant tensors evaluated only once at the simulation initiation.

Note that the mechanical equations (24b) and (24c) correspond to micromorphic (Cosserat) continuum. The primary fields are pressures $p^{(0)}$, displacements $\mathbf{u}^{(0)}$ and rotations $\boldsymbol{\varphi}^{(0)}$. Several emerging coupling terms are obtained describing storage of the fluid in cracks and an effect of volumetric changes on the pressure (Eq. 24a), an effect of the pressure gradient on the linear momentum balance (Eq. 24b), and effects of the pressure gradient and the pressure on the

angular momentum balance (Eq. 24c). The macroscopic equations are naturally anisotropic due to the heterogeneity and cracking at the microscale.

The macroscale problem shall be supplemented with appropriate boundary conditions and solved, e.g., by the finite element method. A transformation of Eqs. (24) to the weak form is straightforward. The macroscopic pressure gradient, $\mathbf{a}$, and the Cosserat strain tensor, $\boldsymbol{\gamma}$, are computed at each integration point and projected onto the RVE problem (Eqs. 20) from which stress-like variables (Eqs. 25) are evaluated.

5 Verification

The *full* and *homogenized* models are implemented in an in-house software. Both steady state and transient simulations are investigated; however, the transient terms are only used for the mass transport part; mechanical behavior is always quasi-static in the presented verification studies. Implicit time integration scheme called the generalized-α method with spectral radius 0.8 is adopted [36, 37]; the two-way coupled problem of mechanical and mass transport balance is solved in a strongly coupled numerical scheme ensuring second order accuracy.

The spatial discretization is based on an actual mesostructure, it shall be called *physical* according to Ref. [23]. All the verification examples assume a material with the maximum aggregate diameter $d_{\max} = 10\,\mathrm{mm}$ and aggregate relative volumetric content 80%. For sake of computational feasibility, only aggregates with diameter above $4\,\mathrm{mm}$ are explicitly considered, the rest is phenomenologically represented by the contact constitutive behavior.

Rezakhani and Cusatis [12] showed that cubic RVE with edge length $5d_{\max}$ is already sufficient for the mechanical problem. According to Ref. [24], such RVE size is acceptable also for the transport problem. Therefore, the RVE used here for all the calculation has size $50 \times 50 \times 50\,\mathrm{mm}^3$; the mechanical RVE has 1539 degrees of freedom (DoF) and the transport RVE has 2160 DoF. A nonlinear steady-state solver is used to calculate the RVE problems.

In the initial intact state, responses of both mechanical and transport RVEs are linear. They can be therefore easily pre-computed resulting in a great computational cost reduction. The linear pre-computed state is adaptively replaced by the full RVE non-linear problem with a help of Ottosen's criterion [38] serving as an indicator of inelastic behavior. The decision process is implemented exactly as described in Ref. [13] for the mechanical homogenization, the transport RVE is replaced simultaneously.

The continuous macroscopic solution is approximated via the finite element method, development of the discretized weak form of Eqs. (24) is straightforward. Cosserat trilinear isoparametric brick elements extended by additional pressure degrees of freedom are used. The same trilinear shape functions are applied to approximate the element shape as well as the displacements, rotations and the pressure. The methodology for element implementation was adopted from Ref. [39]. Full Gauss integration using 8 integration points (hence 8 submodel RVE pairs for each element) is employed.

The model was verified in Ref. [25] by four examples featuring concrete specimens: (i) Terzaghi's consolidation, (ii) flow through a compressed cylinder, (iii) constrained tension of a sealed prism and (iv) hydraulic fracturing of a hollow cylinder. The second and fourth ones are presented also here. They share the same material mesostructure, constitutive model and material parameters (see Ref. [25]).
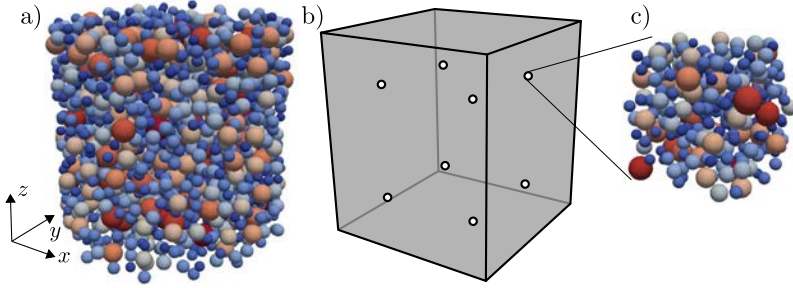
Figure 6: a) Cylindrical specimen, *full* model; b) single brick element, *homogenized* model; c) RVE attached to an integration point.

Flow through compressed cylinder

A steady state simulation of cylinder (depth $0.1\,\mathrm{m}$, diameter $0.1\,\mathrm{m}$) compressed in z direction is performed assuming no friction taking place at the loading platens, i.e., the lateral expansion is completely unconstrained. Simultaneously, a pressure gradient is applied in z direction by prescribing pressure at the bottom face being $1\,\mathrm{MPa}$ and at the top face being $0\,\mathrm{MPa}$. The normal flux component over the curved cylindrical shell is set to zero. The Biot coefficient is $b = 0$, hence this example verifies only a single coupling mechanism, the dependency of the permeability coefficient λ on crack opening.

The *homogenized* model consists of a single brick with 8 integration points. Depth of the brick is $0.1\,\mathrm{m}$, upper and bottom faces are squares of size $0.05\sqrt{\pi} \times 0.05\sqrt{\pi}\,\mathrm{m}^2$ corresponding to the cylinder cross-sectional area. A sketch of the model is shown in Fig. 6. The macroscopic model consists of additional 8 free DoF. The *homogenized* model therefore has $8 \times (2,160 + 2,016) + 8 = 33,416$ DoF in total and runs in $25\,\mathrm{min}$. The *full* model has $32,500$ DoF and runs in $68\,\mathrm{min}$. Even though the number of DoF is similar, the speed-up factor is about 2.7. The improvement is caused by decoupling the systems into separate RVE problems, hence speeding-up its solution.

Stresses and fluxes obtained by the *full* and *homogenized* model are similar, see Fig. 7. Since the constitutive model features strain softening, the mechanical problem suffers from the strain localization. It is well known that localization phenomenon cannot be homogenized as the scale separation does not hold [40]. Few research papers [41, 42] provide suggestions
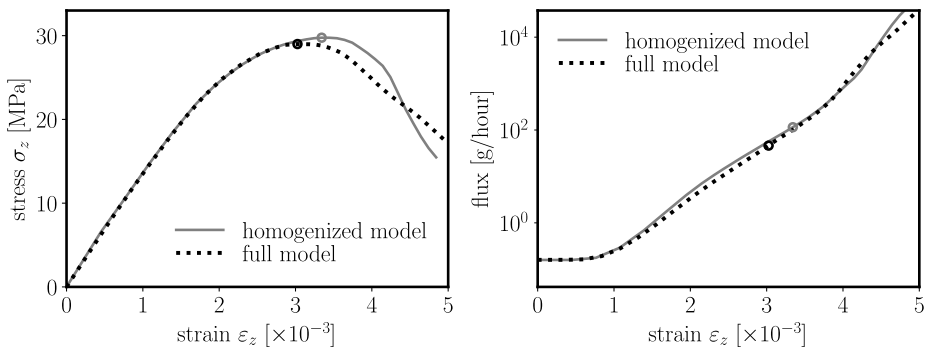
Figure 7: Loading traction and flux through cylindrical specimen obtained by the *full* and *homogenized* model. Circles label states at which the models reached the maximum loading force.

and remedies to capture strain localization properly in the homogenization scheme but these are not implemented here yet. The reason why the verification study gives more or less satisfactory results even with the strain localization is that the RVE volumes exactly correspond to the volumes of material represented by the associated integration points. Consequently, the strain localization occurs in the same material volumes in both models and should be therefore macroscopically equivalent. This shortcut was developed in Ref. [12] for the mechanical problem only, one can see that it is applicable also for the coupled problem. Unfortunately, the major benefit of homogenization, that the large material volume can be macroscopically represented by a small RVE, is lost.

Hydraulic fracturing of hollow cylinder

The second example is meant as a simple application. The specimen is a hollow cylinder of depth $0.05\,\mathrm{m}$, inner radius $r_\mathrm{i} = 0.05\,\mathrm{m}$, outer radius $r_\mathrm{o} = 0.3\,\mathrm{m}$. Cylinder central axis is align with axis z. Transport boundary conditions prescribe constant zero pressure at the outer cylindrical shell, pressure linearly increasing in time $p_\mathrm{i} = 200t$ at the inner surface and zero normal flux at the upper and bottom surfaces at $z = 0\,\mathrm{m}$ and $z = 0.05\,\mathrm{m}$. Mechanical boundary conditions restrict z displacements at the upper and bottom surface and apply an inward traction on the inner surface of magnitude equal to the prescribed pressure.

The *full* model has approximately $323,000\,\mathrm{DoF}$. The *homogenized* model is composed of 4 elements equidistantly distributed in radial direction, 10 elements along the circumference and one element over the depth, resulting in 40 element, 320 RVEs and approx. $320 \times (2,160 + 2,016) \approx 1.3\,\mathrm{mil.\,DoF}$, assuming all the RVEs are switched from pre-computed to inelastic states.

The example features all three coupling fabrics: Biot's effect, storage space created by cracks and permeability enhancement by cracks. Besides full inelastic transient behavior presented here, Eliáš and Cusatis [25] shows additional verification using steady state elastic solution compared with the analytical solution developed in Ref. [43].

The initial and reference pressures are set to zero. Simulation is controlled by increase of the inner pressure, p_i, thus it eventually reaches the critical maximum pressure at which macroscopic cracks develop across the whole cylinder and solver fails due to loss of convergence.
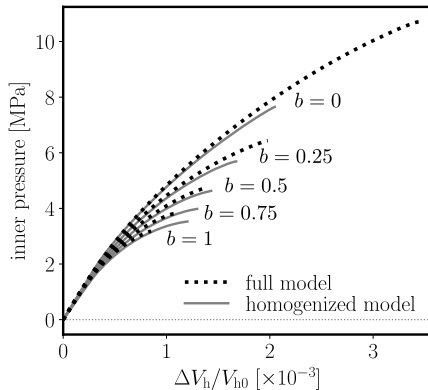
Figure 8: Pressure in the hole obtained during simulation of hydraulic fracturing. The horizontal axis shows relative volumetric change of the central hole of initial volume V_h0, ΔV_h denotes the absolute volume change.
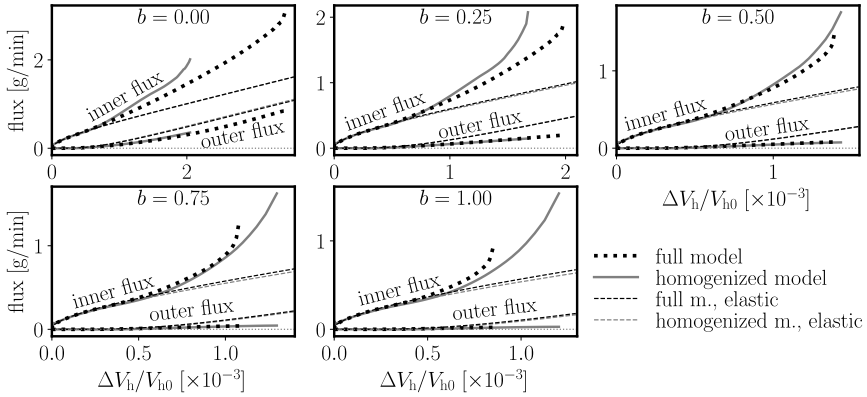
Figure 9: Fluxes obtained during simulation of hydraulic fracturing at the inner and outer cylindrical surface.
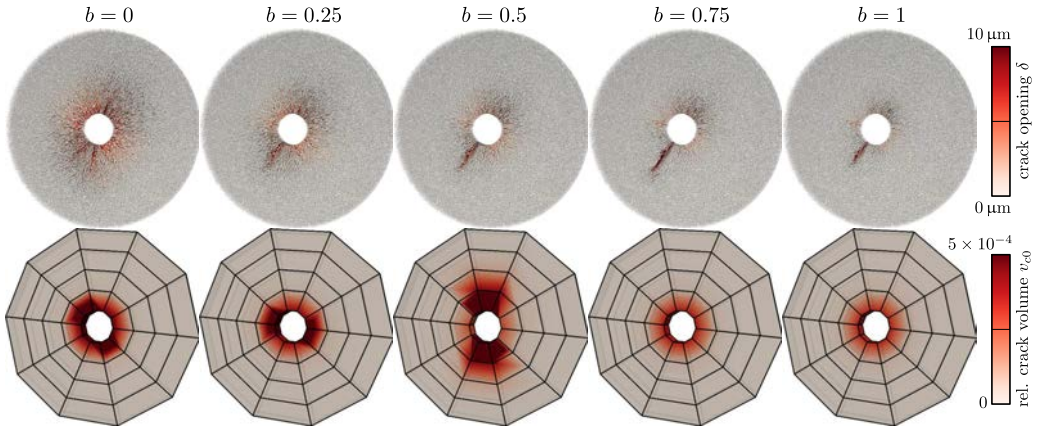
Figure 10: Cracks developed in the *full* and *homogenized* models at the last valid step of the simulation.

Change of volume of the hole, ΔV_{h}, inner flux and outer flux are recorder during the simulation.

The results are shown in Figs. 8 and 9. A reasonable correspondence in terms of pressures/tractions and fluxes is obtained. The larger differences occurring in the later stages of the simulations are attributed to the developed strain localization. The RVE volumes of the *homogenized* model are actually much larger than the the macroscopic material volumes associated with integration points. Unfortunately, the localized cracks significantly affects the solution and cause deviations of the homogenized model results from the reference full solution. Note, that Fig. 9 shows also fluxes obtained from elastic simulations to visualize effect of cracking on the flux as a difference between elastic and inelastic solutions.

Figure 10 shows cracks developed in the *full* and *homogenized* models. One can see localized macrocracks developed in the *full* model. The internal structure of the *full* model (position of particles) is constant, that is why the macrocracks tend to appear at the same locations, presumably at some locally weaker region. On the contrary, the *homogenized* model possesses an ideal symmetry and strain localization occurs in a random direction due to the numerical truncation. No strain localization has been achieved for *homogenized* models with Biot's

coefficients 0.75 and 1, the symmetry was maintained until the last simulation step.

Interestingly enough, the cracking character changes with Biot coefficient. There is more diffused microcracking appearing at the critical pressure around the central hole for low Biot coefficients. This is due to different pressure magnitude sustained by models with different Biot coefficient. If one studies the cracking at the same pressure level, the situation is actually the opposite: larger Biot coefficients give more diffused cracking because the fluid pressure reduces both radial and circumferential compressive stresses in the solid. Since it further helps to open the cracks, the critical pressure for larger Biot coefficients is substantially lower.

The *full* model runs took 2970 min, 2290 min, 1220 min, 980 min and 730 min for Biot coefficients 0, 0.25, 0.5, 0.75 and 1, respectively. Only the coarse *homogenized* model was employed in inelastic analyses reaching computational times 330 min, 250 min, 150 min, 132 min and 120 min and speed-up factors about 9, 9.2, 8.1, 7.4 and 6.1, respectively. This is surprising considering that the *homogenized* model has about 4 times more DoF when all RVEs leave the pre-computed state. The high speed-up factors are achieved by decoupling the system of equations into independent subsystems and also keeping many RVEs in their pre-computed state till the end of the simulation.

6 Coupled Humidity and Heat Conduction

The same homogenization strategy can be applied to discrete mesoscale models of other physical phenomena. Homogenization of a coupled moisture and heat conduction in an idealized dam is presented as was developed in Ref. [24]. Details regarding derivation of the homogenization as well as implementation strategy can be found in the same reference. The Hygro-Thermo-Chemical (HTC) constitutive model and its material parameters were adopted from Refs. [44, 45] to simulate cement hydration and silica fume (pozzolanic) reactions.

The geometry and boundary conditions of the dam are adopted from Gasch et al. [46] and simplified as shown in Fig. 11. The simulated dam has total width of 10.25 m, depth of 13 m and thickness of 1 m, the maximum aggregate diameter is $d_{\max} = 150$ mm. It is assumed that the dam is kept for 2 weeks under moist-curing conditions. After demolding at the end of week 2, it is exposed to the ambient relative humidity and temperature for another 4 weeks before filling with the water and starting its service at the end of week 6.

The boundary conditions during the service life are governed by negative cosine functions with a period of one year for air (a), water (w) and soil (s) temperature (T) and relative humidity (H), see Ref. [24]. The front and back surfaces of the three-dimensional model have prescribed zero out-of-plane flux for both relative humidity and temperature. Also the out-of-plane flux of humidity at the bottom surface is zero. The initial conditions are $T = 15°C$ and $H = 1$ everywhere. The total simulated time is 100 years.

The evolutions of relative humidity and temperature delivered by the *homogenized* model are shown in Fig. 12 in gray color. Three different locations A, B and C are selected for observation. The plotted time range for temperature is shortened as the temperature keeps oscillating in the same manner as in the first six years. Figure 13 shows the relative humidity and temperature profiles along the horizontal line through point B at different time instants. The total computational time of the *homogenized* model was 302 s using 2,246 DoF.

A reasonable estimate is that the *full* model would need months to compute the same analysis. Instead, we simulated only the first 10 years to verify the *homogenized* results. The *full* model has 1,496,652 degrees of freedom, the computational time of the first 10 years was 584,800 s (about one week). The results are shown in Figs. 12 and 13 in black and they agree well with those obtained by the *homogenized* model. The achieved speed-up factor due to
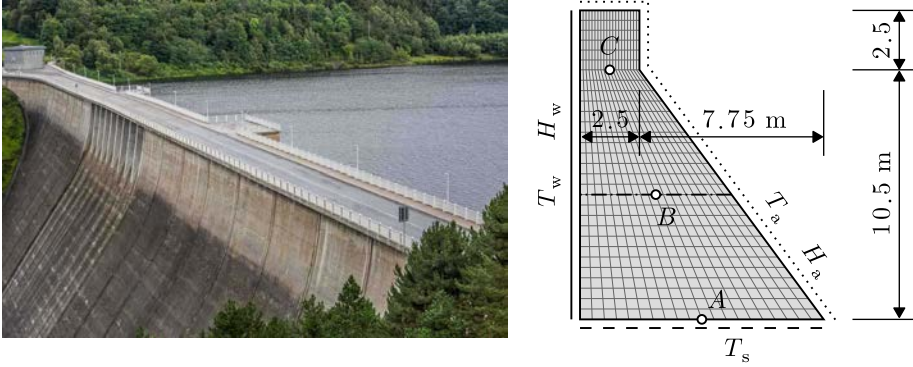
Figure 11: Left: Rappbodetalsperre - an example of a real concrete dam in the Harz Mountains (picture taken from https://www.harz-abenteuer-wandern.de/en/rappbodetalsperre/); right: dimensions and boundary conditions of the idealized dam simulated using coupled heat and moisture conduction.
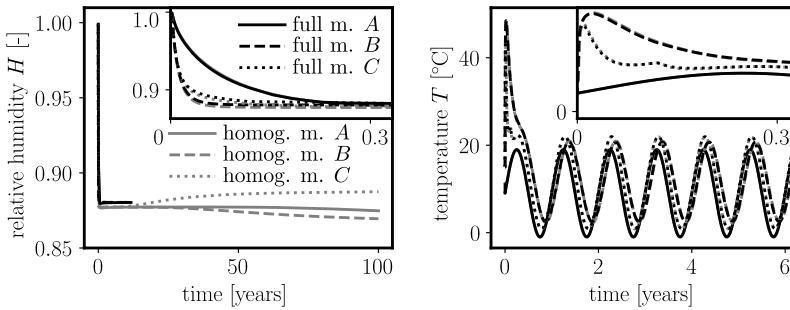
Figure 12: Evolution of relative humidity, and temperature at points A, B and C.
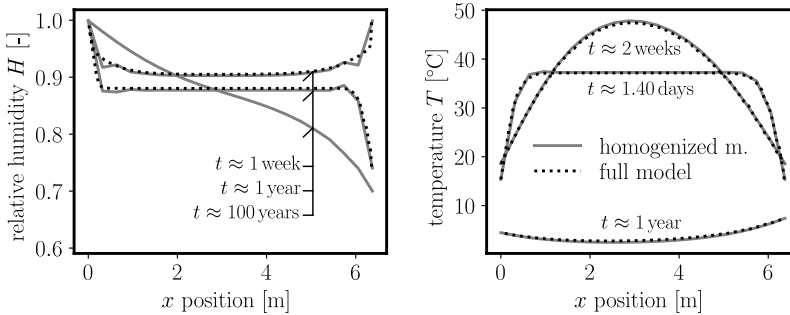
Figure 13: Relative humidity and temperature along the horizontal line through point B.

homogenization is roughly four orders of magnitude. This large speed-up factor is achieved by pre-computing the RVE problem, even though it is strongly nonlinear and with internal sources depending on mathematical description of the cement hydration. The nonlinear part depends on the primary field values (temperature and humidity), which makes the pre-computation possible [24]. The same simplification is unfortunately not applicable in mechanics where the nonlinearity is govern by strain, the first derivative of the primary field.

7 Conclusions

Discrete mesoscale modeling of mechanics, mass transport, heat conduction or coupled processes is a robust and reliable way to predict and asses behavior of concrete structures and structural parts. The main disadvantage is a computational burden associated with the mesoscale character of the model which prohibits wider application in engineering practice. The thesis presents a possible way how to overcame the large computational demands.

Asymptotic expansion homogenization of discrete mesoscale models is developed. A rigorous mathematical derivation is applied for the elastic/linear case while additional realistic assumptions must be utilized for the inelastic/nonlinear case at scale η^{-2}. The macroscale problem arising from the homogenization is described by the standard transient Poisson's equation for the scalar field problems while the mechanical problem results in Cosserat continuous differential equations. Additional coupling terms emerge for coupled problems. The macroscale can be solved with a help of the finite element method with the constitutive equation routines replaced by subscale RVE problems. The macroscopic homogenized material therefore exhibits naturally anisotropy due to heterogeneity and cracking at the microscale.

The microscale (one should say mesoscale in the case of concrete) problems are discrete and steady state. In the case of coupled mechanics and mass transport, the mechanical RVE is independent on the transport RVE while the transport RVE requires information about crack openings from the mechanical RVE. Therefore, they can be solved in a sequence.

The speed-up factor for elastic (and some special inelastic) problems can reach several orders of magnitude because the RVE solution can be pre-computed. Inelastic problems with strain localization unfortunately still requires using the identical material volumes at the macroscale and microscale, therefore the computational savings are relatively low. However, all the calculations are done on a single processor within a single thread. There is a huge potential to speed-up the *homogenized* model by distributing independent RVE problems over several processors. An additional advantage is an extremely simple pre- and post-processing where the standard commercial finite element software can be used (in contrast to the *full* model where special software routines are needed).

Future Activities in Research and Teaching

The main future research plans are focused on improving the homogenization technique and applying it in engineering practice. The following two improvements are planned: (i) further reduction of computational cost via the Proper Orthogonal Decomposition (POD) at the RVE scale and (ii) derivation of a remedy allowing to correctly capture the strain localization within the homogenization scheme.

POD is a model order reduction technique capable to extract a relevant reduced response of a complex system. A high-dimensional problem is projected onto a low-dimensional subspace which contains the solution or at least some good approximation of it. For nonlinear problems the POD subspace is optimal only as long as the model state does not deviate too much from the configuration at which the subspace was built. This is particularly problematic in strain-softening materials where rapid model changes occur when a crack initiates and grows. Therefore the reduced subspace needs to be updated in time as the model nonlinearity evolves. Such an update is quite computationally expensive when done for the whole structure. Kerfriden et al. [10] proposed to use POD only in those parts of the domain where nonlinearity is weak and the update is not needed. Even more elegant would be application of separate PODs for each RVE. The update would be necessary only locally if a substantial evolution of

state variables in the RVE takes place.

The strain localization is the major unsolved problem in multiscale theories as it violates the fundamental homogenization assumptions and the RVE ceases to exist. The microscale problems become size dependent. Recent breakthroughs finally allowed to use homogenization techniques even for quasibrittle materials exhibiting the strain localization. The first crucial progress is development of a special periodic-like boundary conditions [47] capable to initiate and propagate a crack under an arbitrary direction. The second fundamental development is an extension of the homogenization cornerstone, Hill–Mandel principle, for the strain localization. One can, according to Unger [42], duplicate the RVE and solve two RVE problems at the same time after the strain localization occurs at some integration point. The first RVE, loaded by the projection of a localized part of the strain tensor, represents a region with a localized strain. The second RVE, onto which homogeneous part of the strain is projected, represents an unloading region.

An application of the finalized homogenization scheme into engineering practice is planned to be done in connection with company DesignTec. They are experienced in complex numerical analysis of structures using Ansys software. We would like to implement the RVE analysis into Ansys as a material constitutive equation subroutine. Consequently, the whole discrete mesoscale model would appear to the user only as a different material in otherwise standard calculation setup.

Other author's future research directions are relatively broad, from general mechanics of solids to coupled multi-physical problems, high strain rate events and blending mechanics and probability theory. These topics are intensively studied by scholars around the world. The author would like to strengthen his international collaboration in these fields, work further with the current international connections and find new contacts and opportunities abroad.

The fundamental ingredient to fulfill these ambitious plans is a collaboration with motivated and talented students at the Institute of Structural Mechanics in Brno. The author sees the basic teaching activities as a crucial part of his work assignment that may recruit talented students for Ph.D. programs. There are currently two young Ph.D. students working with the author on these topics and there is definitely enough room for some more local or international applicants.

References

[1]   Zdeněk P. Bažant and Byung Hwan Oh. "Crack band theory for fracture of concrete". *Matériaux et Construction* 16 (1983), 155–177. ISSN: 0981-5406. DOI: 10.1007/BF02486267.

[2]   Nicolas Moës, John Dolbow, and Ted Belytschko. "A finite element method for crack growth without remeshing". *International Journal for Numerical Methods in Engineering* 46.1 (1999), 131–150. DOI: 10.1002/(SICI)1097-0207(19990910)46:1<131::AID-NME726>3.0.CO;2-J.

[3]   Milan Jirásek. "Nonlocal models for damage and fracture: Comparison of approaches". *International Journal of Solids and Structures* 35.31 (1998), 4133–4145. ISSN: 0020-7683. DOI: 10.1016/S0020-7683(97)00306-5.

[4]   Blaise Bourdin, Gilles A. Francfort, and Jean-Jacques Marigo. "The Variational Approach to Fracture". *Journal of Elasticity* 91 (2008), 5–148. DOI: 10.1007/s10659-007-9107-3.

[5]   Gianluca Cusatis, Daniele Pelessone, and Andrea Mencarelli. "Lattice Discrete Particle Model (LDPM) for failure behavior of concrete. I: Theory". *Cement and Concrete Composites* 33.9 (2011), 881–890. ISSN: 0958-9465. DOI: 10.1016/j.cemconcomp.2011.02.011.

[6]   Gianluca Cusatis, Andrea Mencarelli, Daniele Pelessone, and James Baylot. "Lattice discrete particle model (LDPM) for failure behavior of concrete. II: Calibration and validation". *Cement and Concrete composites* 33.9 (2011), 891–905.

[7] John E. Bolander, T. Shiraishi, and Y. Isogawa. "An adaptive procedure for fracture simulation in extensive lattice networks". *Eng Fract Mech* 53.3 (1996), 325–334. ISSN: 0013-7944. DOI: 10.1016/0013-7944(95)00200-6.

[8] Alejandro Cornejo, Vicente Mataix, Francisco Zárate, and Eugenio Oñate. "Combination of an adaptive remeshing technique with a coupled FEM-DEM approach for analysis of crack propagation problems". *Computational Particle Mechanics* 7 (2020), 735–752. DOI: 10.1007/s40571-019-00306-4.

[9] Erol Lale, Roozbeh Rezakhani, Mohammed Alnaggar, and Gianluca Cusatis. "Homogenization coarse graining (HCG) of the lattice discrete particle model (LDPM) for the analysis of reinforced concrete structures". *Engineering Fracture Mechanics* 197 (2018), 259–277. ISSN: 0013-7944. DOI: 10.1016/j.engfracmech.2018.04.043.

[10] Pierre Kerfriden, Jean-Charles Passieux, and Stéphane Pierre Alain Bordas. "Local/global model order reduction strategy for the simulation of quasi-brittle fracture". *International Journal for Numerical Methods in Engineering* 89.2 (2012), 154–179. DOI: https://doi.org/10.1002/nme.3234.

[11] Chiara Ceccato, Xinwei Zhou, Daniele Pelessone, and Gianluca Cusatis. "Proper Orthogonal Decomposition Framework for the Explicit Solution of Discrete Systems With Softening Response". *Journal of Engineering Mechanics* 85.5 (2018), 051004. DOI: 10.1115/1.4038967.

[12] Roozbeh Rezakhani and Gianluca Cusatis. "Asymptotic expansion homogenization of discrete fine-scale models with rotational degrees of freedom for the simulation of quasi-brittle materials". *Journal of the Mechanics and Physics of Solids* 88 (2016), 320–345. ISSN: 0022-5096. DOI: 10.1016/j.jmps.2016.01.001.

[13] Roozbeh Rezakhani, Xinwei Zhou, and Gianluca Cusatis. "Adaptive multiscale homogenization of the lattice discrete particle model for the analysis of damage and fracture in concrete". *International Journal of Solids and Structures* 125 (2017), 50–67. ISSN: 0020-7683. DOI: h10.1016/j.ijsolstr.2017.07.016.

[14] Gianluca Cusatis, Roozbeh Rezakhani, and Edward A. Schauffert. "Discontinuous Cell Method (DCM) for the simulation of cohesive fracture and fragmentation of continuous media". *Engineering Fracture Mechanics* 170 (2017), 1–22. ISSN: 0013-7944. DOI: 10.1016/j.engfracmech.2016.11.026.

[15] Daisuke Asahina, Kazuhei Aoyagi, Kunhwi Kim, Jens T. Birkholzer, and John E. Bolander. "Elastically-homogeneous lattice models of damage in geomaterials". *Computers and Geotechnics* 81 (2017), 195–206. ISSN: 0266-352X. DOI: 10.1016/j.compgeo.2016.08.015.

[16] Jan Eliáš and Henrik Stang. "Lattice Modeling of Aggregate Interlocking in Concrete". *International Journal of Fracture* 175 (2012), 1–11. ISSN: 0376-9429. DOI: 10.1007/s10704-012-9677-3.

[17] Jan Eliáš, Petr Frantík, and Miroslav Vořechovský. "Improved sequentially linear solution procedure". *Engineering Fracture Mechanics* 77.12 (2010), 2263–2276. ISSN: 0013-7944. DOI: 10.1016/j.engfracmech.2010.05.018.

[18] Jan Eliáš, Miroslav Vořechovský, Jan Skoček, and Zdeněk P. Bažant. "Stochastic discrete meso-scale simulations of concrete fracture: comparison to experimental data". *Engineering Fracture Mechanics* 135 (2015), 1–16. ISSN: 0013-7944. DOI: 10.1016/j.engfracmech.2015.01.004.

[19] Jan Eliáš and Miroslav Vořechovský. "Fracture in random quasibrittle media: I. Discrete mesoscale simulations of load capacity and fracture process zone". *Engineering Fracture Mechanics* 235 (2020), 107160. ISSN: 0013-7944. DOI: 10.1016/j.engfracmech.2020.107160.

[20] Jan Eliáš. "Elastic properties of isotropic discrete systems: Connections between geometric structure and Poisson's ratio". *International Journal of Solids and Structures* 191-192 (2020), 254–263. ISSN: 0020-7683. DOI: 10.1016/j.ijsolstr.2019.12.012.

[21] Jan Eliáš. "Boundary Layer Effect on Behavior of Discrete Models". *Materials* 10 (2017), 157. ISSN: 1996-1944. DOI: 10.3390/ma10020157.

[22] Jan Eliáš. "Adaptive technique for discrete models of fracture". *International Journal of Solids and Structures* 100–101 (2016), 376–387. ISSN: 0020-7683. DOI: 10.1016/j.ijsolstr.2016.09.008.

[23] John E. Bolander, Jan Eliáš, Gianluca Cusatis, and Kohei Nagai. "Discrete mechanical models of concrete fracture". *Engineering Fracture Mechanics* 257 (2021), 108030. ISSN: 0013-7944. DOI: 10.1016/j.engfracmech.2021.108030.

[24] Jan Eliáš, Hao Yin, and Gianluca Cusatis. "Homogenization of discrete diffusion models by asymptotic expansion". *International Journal for Numerical and Analytical Methods in Geomechanics* (2022). under review. ISSN: 0363-9061.

[25] Jan Eliáš and Gianluca Cusatis. "Homogenization of discrete mesoscale model of concrete for coupled mass transport and mechanics by asymptotic expansion". *Journal of the Mechanics and Physics of Solids* (2022). under review. ISSN: 0022-5096.

[26] William B. Fuller and Sanford E. Thompson. "The Laws of Proportioning Concrete". *Transactions of the American Society of Civil Engineers* 59.2 (1907), 67–143. DOI: 10.1061/TACEAT.0001979.

[27] Peter Grassl. "A lattice approach to model flow in cracked concrete". *Cement and Concrete Composites* 31.7 (2009), 454–460. ISSN: 0958-9465. DOI: 10.1016/j.cemconcomp.2009.05.001.

[28] Peter Grassl and John Bolander. "Three-Dimensional Network Model for Coupling of Fracture and Mass Transport in Quasi-Brittle Geomaterials". *Materials* 9.9 (2016), 782. ISSN: 1996-1944. DOI: 10.3390/ma9090782.

[29] Daisuke Asahina, Pengzhi Pan, Kimikazu Tsusaka, Mikio Takeda, and John E. Bolander. "Simulating hydraulic fracturing processes in laboratory-scale geological media using three-dimensional TOUGH-RBSN". *Journal of Rock Mechanics and Geotechnical Engineering* 10.6 (2018), 1102–1111. ISSN: 1674-7755. DOI: 10.1016/j.jrmge.2018.09.001.

[30] Ignatios Athanasiadis, Simon J. Wheeler, and Peter Grassl. "Hydro-mechanical network modelling of particulate composites". *International Journal of Solids and Structures* 130-131 (2018), 49–60. ISSN: 0020-7683. DOI: 10.1016/j.ijsolstr.2017.10.017.

[31] Weixin Li, Xinwei Zhou, J. William Carey, Luke P. Frash, and Gianluca Cusatis. "Multiphysics Lattice Discrete Particle Modeling (M-LDPM) for the Simulation of Shale Fracture Permeability". *Rock Mechanics and Rock Engineering* 51 (2018), 3963–3981. ISSN: 0723-2632. DOI: 10.1007/s00603-018-1625-8.

[32] Maurice A. Biot. "General Theory of Three-Dimensional Consolidation". *Journal of Applied Physics* 12.2 (1941), 155–164. DOI: 10.1063/1.1712886.

[33] Emmanuel Detournay and Alexander H.-D. Cheng. "Comprehensive Rock Engineering: Principles, Practice & Projects". In: vol. II. 1995, 113–171. DOI: 10.1016/B978-0-08-040615-2.50011-3.

[34] Gianluca Cusatis and Luigi Cedolin. "Two-scale study of concrete fracturing behavior". *Engineering Fracture Mechanics* 74.1 (2007). Fracture of Concrete Materials and Structures, 3–17. ISSN: 0013-7944. DOI: 10.1016/j.engfracmech.2006.01.021.

[35] Jacob Fish, Wen Chen, and Renge Li. "Generalized mathematical homogenization of atomistic media at finite temperatures in three dimensions". *Computer Methods in Applied Mechanics and Engineering* 196.4 (2007), 908–922. ISSN: 0045-7825. DOI: 10.1016/j.cma.2006.08.001.

[36] Sandra Carstens and Detlef Kuhl. "Higher-order accurate implicit time integration schemes for transport problems". *Archive of Applied Mechanics* 82.8 (2012), 1007–1039. ISSN: 1432-0681. DOI: 10.1007/s00419-012-0638-0.

[37] Kenneth E. Jansen, Christian H. Whiting, and Gregory M. Hulbert. "A generalized-α method for integrating the filtered Navier–Stokes equations with a stabilized finite element method". *Computer Methods in Applied Mechanics and Engineering* 190.3 (2000), 305–319. ISSN: 0045-7825. DOI: 10.1016/S0045-7825(00)00203-6.

[38] Niels Saabye Ottosen. "A Failure Criterion for Concrete". *Journal of the Engineering Mechanics Division ASCE* 103 (1977), 527–535. ISSN: 0044-7951. DOI: 10.1061/JMCEA3.0002248.

[39] Martin Horák, Bořek Patzák, and Milan Jirásek. "On design of element evaluators in OOFEM". *Advances in Engineering Software* 72 (2014), 193–202. ISSN: 0965-9978. DOI: 10.1016/j.advengsoft.2014.01.006.

[40] Inna M. Gitman, Harm Askes, and Lambertus J. Sluys. "Representative volume: Existence and size determination". *Engineering Fracture Mechanics* 74.16 (2007), 2518–2534. ISSN: 0013-7944. DOI: 10.1016/j.engfracmech.2006.12.021.

[41] Erica W.C. Coenen, Varvara G. Kouznetsova, E. Bosco, and Marc G.D. Geers. "A multi-scale approach to bridge microscale damage and macroscale failure: a nested computational homogenization-localization framework". *International Journal of Fracture* 178 (2012), 157–178. DOI: 0.1007/s10704-012-9765-4.

25

[42]   Jörg F. Unger. "An FE2-X1 approach for multiscale localization phenomena". *Journal of the Mechanics and Physics of Solids* 61.4 (2013), 928–948. ISSN: 0022-5096. DOI: 10.1016/j.jmps.2012.12.010.

[43]   Peter Grassl, Caroline Fahy, Domenico Gallipoli, and S.J. Wheeler. "On a 2D hydro-mechanical lattice approach for modelling hydraulic fracture". *Journal of the Mechanics and Physics of Solids* 75 (2015), 104–118. ISSN: 0022-5096. DOI: 10.1016/j.jmps.2014.11.011.

[44]   Giovanni Di Luzio and Gianluca Cusatis. "Hygro-thermo-chemical modeling of high performance concrete. I: Theory". *Cement and Concrete Composites* 31.5 (2009), 301–308. ISSN: 0958-9465. DOI: 10.1016/j.cemconcomp.2009.02.015.

[45]   Giovanni Di Luzio and Gianluca Cusatis. "Hygro-thermo-chemical modeling of high-performance concrete. II: Numerical implementation, calibration, and validation". *Cement and Concrete Composites* 31.5 (2009), 309–324. ISSN: 0958-9465. DOI: 10.1016/j.cemconcomp.2009.02.016.

[46]   Tobias Gasch, Richard Malm, and Anders Ansell. "A coupled hygro-thermo-mechanical model for concrete subjected to variable environmental conditions". *International Journal of Solids and Structures* 91 (2016), 143–156.

[47]   Erica W.C. Coenen, Varvara G. Kouznetsova, and Marc G.D. Geers. "Novel boundary conditions for strain localization analyses in microstructural volume elements". *International Journal for Numerical Methods in Engineering* 90.1 (2012), 1–21. DOI: 10.1002/nme.3298.

Abstract

Mechanics and mass transport phenomena in concrete structures are strongly coupled. The first coupling fabric is the Biot's theory according to which fluid pressure interacts with solid stress state and volumetric deformation rate of the solid induces changes in fluid pressure. Another coupling mechanism emerges with cracks which serve as opens channels for the fluid to flow through them. Especially the second coupling mechanism presents a challenge for numerical modeling as it requires detailed knowledge about cracking process. Discrete mesoscale mechanical models coupled with mass transport offer simple and robust way to solve the problem.

The kinematics of the discrete model is based on polyhedral rigid bodies interconnected by compliant contacts. There is a vectorial constitutive relation at the interparticle contact lumping together both elastic and inelastic parts of the material behavior. Thanks to discrete displacement jumps between rigid particles, the cracks are naturally represented and oriented. Mesoscale character of the model ensures high-fidelity of the crack pattern. On the other hand, detailed mesoscale representation lead to large computational demands.

Asymptotic expansion homogenization technique for the discrete coupled problem is developed in order to reduce this computational burden. It delivers (i) continuous and homogeneous description of the macroscopic problem which can be easily solved by the finite element method, (ii) discrete and heterogeneous mesoscale problem in the periodic setup attached to each integration point of the macroscale along with (iii) equations providing communication between these two scales. The transient terms appear at the macroscale only, as well as the Biot's coupling terms. The coupling through cracking is treated at the mesoscale by changing conductivity of the conduit elements according to the mechanical solution, otherwise the two mesoscale steady state problems are decoupled and can be therefore solved in a sequence. Verification studies showing performance of the homogenized solution are presented as well.

Homogenization of coupled heat and humidity conduction is presented in the last section and verified by simulating large concrete dam in a fraction of time needed by the original mesoscale model.

Shrnutí

Autor se dlouhodobě věnuje výzkumu v oblasti výpočtové mechaniky. Jeho hlavním výzkumným tématem je vývoj diskrétních mesoúrovňových modelů mechanického porušení betonu. V předložené práci jsou představeny výsledky vytvořené přibližně v posledním roce a půl ve spolupráci s prof. Gianlucou Cusatisem z Northwestern University, Illinois USA, které jsou v tuto chvíli (květen 2022) zaslány k recenznímu řízení do impaktovaných časopisů. Tyto výsledky ukazují analytické odvození homogenizovaného řešení diskrétního mesoúrovňového modelu pro sdruženou úlohu mechaniky a transportu hmoty v betonu. Hlavním cílem tohoto výzkumu je snížit výpočtovou náročnost diskrétního modelu a výrazně zjednodušit práci s ním (přípravu modelu a vyhodnocení výsledků). Výhledově je takovéto homogenizované řešení vhodné pro implementaci v komerčních softwarech jako materiálová (konstitutivní) funkce volaná v každém integračním bodě konečněprvkového modelu.

Diskrétní mesoúrovňový model je v současné době ve světě považován za jeden z nejrobustnějších numerických modelů pro simulace porušení betonu. Diskrétní popis pole posunů redukuje počet stupňů volnosti modelu a také umožňuje jednoduchou reprezentaci orientovaných trhlin v materiálu. Mimo to podstatně zjednodušuje řídicí rovnice, které již nemají charakter parciálních diferenciálních rovnic, a konstitutivní vztahy. Ty jsou ve spojitých

modelech formulovány tenzorově a vyžadují nezávislost na rotaci souřadnicového systému, v diskrétních modelech jsou to jednodušší, pouze vektorové vztahy. Díky tomu, že mesoúrovňový model přímo obsahuje materiálovou strukturu betonu (zrna kameniva, matrici, případně póry), je v modelu automaticky zohledněna charakteristická délka materiálu a také se objevují oscilace v poli napětí a deformace odpovídající heterogennímu charakteru materiálu. Tyto oscilace umožňují například vznik příčných tahových trhlin při tlakovém zatěžování. Řada vědeckých článků ukazuje validaci těchto modelů pomocí různých druhů experimentů.

Díky věrnému popisu trhlin jsou diskrétní mesoúrovňové modely vhodné pro sdružené úlohy, kdy se současně simuluje několik provázaných fyzikálních jevů. V případě této práce se jedná o provázaný problém mechaniky a transportu tekutin, tzv. poromechaniku. V elastické oblasti je provázání těchto dvou problémů popsáno pomocí Biotovy teorie, při vzniku trhlin se přidávají další sdružující jevy jako ukládání tekutiny v prostoru trhlin nebo snadný tok kapaliny vytvořenými trhlinami. Proto je důležité dosáhnout v mechanickém modelu realistické reprezentace trhlin, jejich množství, otevření a orientace.

Kritickou nevýhodou všech mesoúrovňových (nejen diskrétních) modelů je ovšem jejich výpočtová náročnost. Jelikož je jejich diskretizace řízena velikostí materiálových heterogenit, bývá náročné simulovat už i některá větší laboratorní betonová tělesa, natož celé konstrukční dílce. Existují různé techniky umožňující ušetřit výpočtový čas, například pomocí adaptivní diskretizace nebo sofistikované projekce problému do podprostoru s méně stupni volnosti. Jednou z nejuniverzálnějších cest, jak ušetřit výpočtový čas, je však u heterogenních materiálů homogenizace.

Tato práce představuje odvození homogenizační techniky pro diskrétní modely sdružené úlohy mechaniky a transportu. Nejprve je provedeno rozdělení primárních veličin diskrétního modelu na dvě složky: makroúrovňovou, představující průměrné chování, a mikroúrovňovou, představující periodické oscilace okolo průměru. Toho je dosaženo přidáním velmi malé konstanty η, která vyjadřuje úroveň, na které se jednotlivé výrazy nacházejí. Druhou zásadní ingrediencí je aproximace primárních veličin mezi sousedními diskrétními zrny pomocí Taylorovy řady. Tyto dvě fundamentální složky jsou vloženy do řídicích rovnic modelu, které se následně rozpadnou do několika úrovní podle mocniny konstanty η. Získané sady řídicích rovnic pak popisují numerický problém na dvou různých úrovních. Makroúrovňový model je spojitý a homogenní. Je popsán parciálními diferenciálními rovnicemi Cosseratova typu, které je možné, po převedení na slabou formulaci, řešit pomocí metody konečných prvků. Makroúroveň obsahuje časově závislé výrazy (transientní problém). Oproti tomu je mikroúroveň diskrétní, heterogenní a statická, časová proměnná v rovnicích nevystupuje. Je představována dvěma periodickými problémy, jedním pro mechaniku a jedním pro transport. Zatížení mikroúrovňových periodických úloh je vnášeno projekcí makroskopického tenzoru deformace a vektoru gradientu tlaku. Výsledky z mikroúrovně jsou pak přeneseny zpět na makroúroveň jako tenzory napětí a vektor toku.

Sdružující členy představující Biotovu teorii a ukládání tekutiny v trhlinách jsou přítomny pouze na makroúrovni. Vliv trhlin na propustnost materiálu se však projevuje na mikroúrovni. Nejprve je nutné vyřešit mechanický periodický problém, získané otevření trhlin poté přenést do transportního periodického problému a následně ho vyřešit.

Práce ukazuje příklady porovnávající homogenizované a plné řešení, tedy řešení vypočtené s původním diskrétním mesoúrovňovým modelem. V naprosté většině případů je dosaženo dobré shody a zásadní úspory výpočtového času. V případech, kdy dochází k lokalizaci deformace, však nejsou splněny předpoklady pro homogenizaci a vznikají odchylky od plného řešení. Úprava homogenizovaného modelu tak, aby pokrýval i lokalizaci deformace, je podle současné vědecké literatury možná, a bude předmětem dalšího výzkumu autora práce.